Fourth International MeetingonWind Turbine Noise

Rome Italy 12-14 April 2011

CFD Analysis of the Influence of Central Shaft on Vertical-Axis Wind Turbine Noise Emission

Marco Raciti Castelli (*), Alberto Villa, Ernesto Benini (**)

Department of Mechanical Engineering – University of Padova
Via Venezia, 1 – 35131 Padova, Italy
(*) marco.raciticastelli@unipd.it, (**) ernesto.benini@unipd.it

Abstract

This paper presents the results of two-dimensional CFD simulations of the flow field around a vertical-axis wind turbine rotor, with emphasys on noise generation and propagation. The effect of the central shaft on overall rotor noise emission is analyzed using the Ffowcs-Williams and Hawkings acoustic model.

The solutions are obtained using unstructured moving sub-grids rotating along with the rotor blades. After describing and validating the computational model with experimental data, a time-accurate flow solution is generated for two different rotor configurations, characterized by a simple NACA 0021 three-bladed rotor and by a NACA 0021 three-bladed rotor presenting a central shaft.

After running transient solutions until statistically steady-states are obtained by monitoring the major flow field and dynamic variables (such as rotor instantaneous torque), 8 acoustic receivers are placed inside the computational domain and their sound pressure signals are analyzed as a function of both time and rotor angular position.

Flow field characteristics are investigated for optimum tip speed ratio conditions, allowing a first estimation of the influence of the central shaft on vertical-axis wind turbine sound emission.

Nomenclature

A_s [mm2]	rotor swept area
c [mm]	blade chord
$C_{p,ave}$ [-]	average power coefficient during a full rotor revolution
$C_T(\theta)$ [-]	rotor instantaneous torque coefficient
D_{rotor} [mm]	rotor diameter

D_{shaft} [mm]	shaft diameter
f [Hz]	acoustic pulsation frequency due to interference between blades and shaft wake
H_{rotor} [mm]	rotor height
L_x [mm]	distance from rotor axis in the direction of unperturbed freestream
L_w [dB]	acoustic power level
N [-]	number of rotor blades
p [Pa]	sound pressure
p_{ref} [Pa]	reference sound pressure (assumed 2·10-5)
P_{ave} [W]	average power during a full rotor revolution
R_{rotor} [m]	rotor radius
T [s]	rotor period of revolution
T_{rotor} (θ) [Nm]	rotor instantaneous torque
TSR [-]	tip speed ratio
V_∞ [m/s]	unperturbed wind velocity at computational domain entrance
W_0 [W]	reference sound power level (assumed 10-12)
W_{sound} [W]	sound power
θ [°]	blade azimuthal coordinate
ρ [kg/m3]	air density (assumed 1.225)
σ [-]	rotor solidity
ω[rad/s]	rotor angular velocity

Introduction

The urgent need to reduce dependence on fossil fuels is being met, at least in part, by the development of wind turbines, both onshore and offshore: the awareness of the limited resources of fossil fuels and the rising concern for the effects of the increased amount of greenhouse gases in the atmosphere have given the wind turbine industry a considerable push forward. As pointed out by the First International Conference on Wind Turbine Noise [1], the development of onshore wind power results in wind turbines closer to habitations, leading to the possibility of noise problems, such that frequent objections raised in planning procedures concern noise and vibration.

In recent years a growing interest in the use of wind turbines inside urban areas is also to be registered. Due to the unpredictability and unsteadiness of the airflow close to buildings, conventional horizontal-axis wind turbine (HAWT) designs resulted in low efficiency because of their requirement to be set into the wind direction in

order to operate at maximum power coefficient. Thanks to its inherent capability of operating independently from wind direction, an effective alternative is a vertical-axis design, which has now reached first-generation production level. Moreover, vertical-axis wind turbine (VAWT) maximum power coefficient can be obtained at lower tip-speed ratio compared with conventional HAWTs, thus reducing flow induced noise. However, little is known about such turbine noise generation. Hence, as stated by Sezer-Uzol et al. [2], the accurate predictions of aerodynamic loads and noise become a challenging key issue in the design process of wind turbines, in consideration of their intended locations. VAWT designers result therefore in need of guidance to ensure that their products have satisfactory acoustic performance. As reported by Pedersen [3], on the one hand, there is a social requirement for erecting more wind turbines in order to generate electricity without harm to the environment; on the other hand, there is an individual need for quiet and peace in the home environment: both these demands have to be met in the future developments of wind turbine design.

Computational Fluid Dynamics (CFD) can nowadays be considered as a powerful design tool, whose integration into industrial development and production life-cycles is continuously rising. As observed by Caridi [4], this was made possible because of two main factors:

- the increase in computer performance and network facilities;
- the progress made in general purpose CFD software between modeling complexity and practicability within the industrial environment.

Nevertheless, while numerical methodologies are well established for several applications such as aerodynamics, heat exchange, etc., aeroacoustic CFD simulations still represent a challenge, in particular as far as their industrial practicability is concerned.

Timouchev [5] performed three-dimensional CFD analysis of a 2 m diameter and 4.03 m height Savonius rotor characterized by a twisted double-bladed architecture for a wind velocity of 10 m/s. The numerical simulations showed that the non-uniformity of the flow-field generated by the interaction between the freestream and the Savonius turbine blades generates blade passing frequencies (BPF) pressure pulsations, whose amplitudes attenuate very rapidly inside a zone of about 15 rotor diameters from the noise source.

Iida et al. [6] simulated the unsteady flow field around a three-bladed Darrieus rotor adopting the discrete vortex method. The aerodynamic noise radiated from the turbine, estimated at 5 m distance from the rotor axis, was determined using the Ffowcs Williams-Hawkings method [7]. The numerical results showed the reduced noise emission of a VAWT compared to a classical horizontal-axis configuration, indicating VAWTs as useful candidates in order to develop low-noise power generation systems.

The present work proposes the results of two-dimensional, time-accurate, parallel CFD simulations of the flow field around a three-bladed Darrieus rotor. *Realizable k-ε* turbulence model with *Enhanced Wall Treatment* option is used for viscous computations. The commercial 2-D, unsteady, parallel, finite volume flow solver ANSYS FLUENT ® is used for the simulations. The solutions are obtained using

unstructured moving grids rotating with the turbine blades. Two different flow cases are investigated:

- a three-bladed configuration without central shaft, named *Model 0*;
- the same rotor architecture in presence of the central shaft, named *Model 1*.

The effect of the central shaft on overall rotor noise emission is thus analyzed, using the Ffowcs-Williams and Hawkings acoustic model, by means of 8 receivers placed inside the computational domain, whose sound pressure signals are analyzed as a function of both time and rotor angular position.

Model Geometry

The aeroacoustic analysis proposed in the present work is based upon the 2D vertical-axis Darrieus wind turbine geometry analyzed by RacitiCastelli et al. [8], [9]. Rotor's main geometrical features are summarized in Table 1. The solidity parameter σ is defined as Nc/R_{rotor}, as suggested by Strickland [10].

D_{rotor} [mm]	1030
H_{rotor} [mm]	1 (2D simulation)
N [-]	3
Blade profile	NACA 0021
c [mm]	85.8
Spoke-blade connection	0.25 c
σ [-]	0.5
D_{shaft} [mm]	50

Table 1: Main geometrical features of the tested models

Rotor azimuthal position was identified by the angular coordinate of the pressure centre of blade No. 1 midsection (set at 0.25·c for NACA 0021 airfoil), starting between the 2nd and 3rd cartesian plane octants, as can be seen in Figure 1.

The aeroacoustic analysis was conducted for the turbine operating inside a constant wind speed of 9 m/s and for an optimum tip speed ratio, defined as:

$$TSR = \omega R_{rotor} / V_\infty \quad (1)$$

of 2.33, as can be determined from Figure 2, representing the evolution of rotor average power coefficient, defined as:

$$C_{p,ave} = \frac{P_{ave}}{1/2\,\rho\, A_s\, V_\infty^{\,3}} \qquad (2)$$

as a function of the TSR parameter.

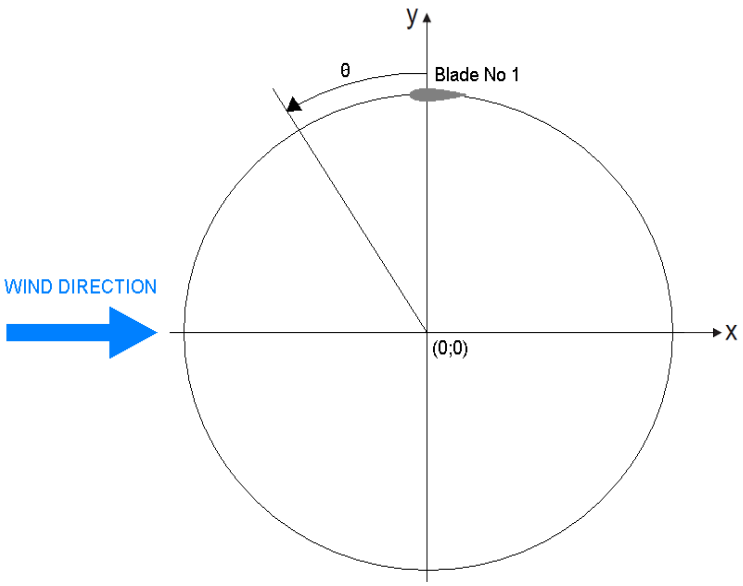

Figure 1: Azimuthal coordinate of blade midsection's centre of pressure (from: [8])

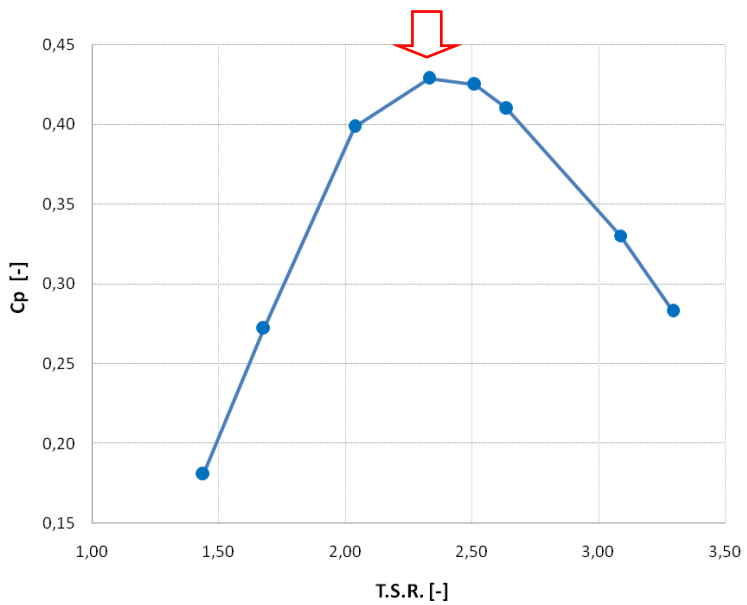

Figure 2: Evolution of rotor average power coefficient as a function of TSR for an incident wind speed of 9 m/s (from: [8]); the red arrow indicates the optimum TSR position, where the aeroacoustic analysis was conducted

Spatial Domain Discretization

The use of moving sub-grids was necessary, due to the movement of the rotor elements. In particular, the discretization of the computational domain into macro-areas has led to two distinct sub-grids:

- a rectangular outer zone, determining the overall calculation domain, with a circular opening centered on the turbine rotational axis, which was identified as *Wind Tunnel sub-grid*, fixed;
- a circular inner zone, which was identified as *Rotor sub-grid*, rotating with rotor angular velocity ω.

Wind Tunnel Sub-Grid

Figure 3 shows the main dimensions and the boundary conditions of the *Wind Tunnel sub-grid* area.

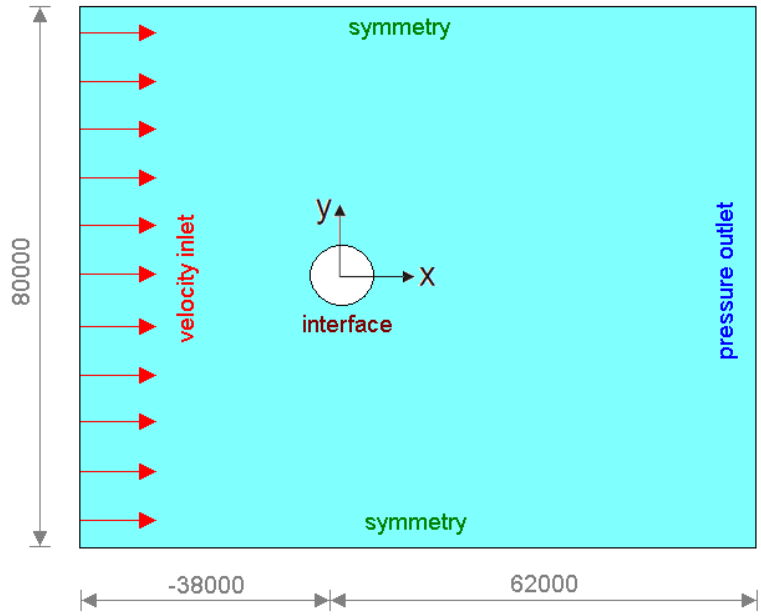

Figure 3: Main dimensions [mm] of the *Wind Tunnel sub-grid* area (from: [8])

Two *symmetry* boundary conditions were used for the two side walls. The circumference around the circular opening centered on the turbine rotational axis was set as an *interface*, thus ensuring the continuity in the flow field.

An unstructured mesh was chosen for the *Wind Tunnel sub-grid*, in order to reduce engineering time to prepare the CFD simulations.

RotorSub-Grid

The *Rotor sub-grid* is the fluid area simulating the revolution of the wind turbine and is therefore characterized by a moving mesh, rotating at the same angular velocity of

the turbine. Its location coincides exactly with the circular opening inside the *Wind Tunnel sub-grid* area and is centred on the turbine rotational axis.

Figure 4 shows the main dimensions and the boundary conditions of the *Rotor sub-grid* area.

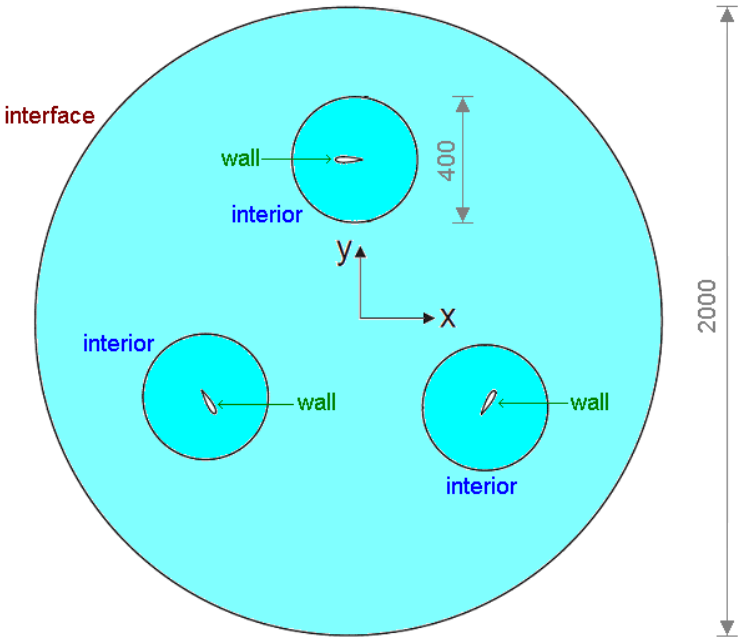

Figure 4: Schema of *Rotor sub-grid* main dimensions [mm] (from: [8])

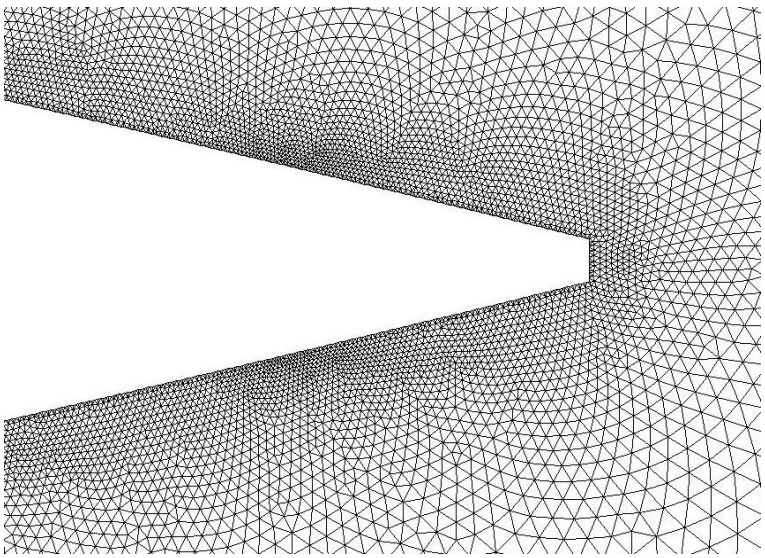

Figure 5: Grid points clustering close to trailing edge (from: [9])

An isotropic unstructured mesh was chosen for the *Rotor sub-grid*, in order to test the prediction capability of a very simple grid. All blade profiles inside the *Rotor sub-grid* area are enclosed in a control circle of 400 mm diameter. Unlike the *interface*, it has

no physical significance: its aim is to allow a precise dimensional control of the grid elements in the area close to rotor blades by adopting a first *size function* operating from the blade profile to the control circle itself and a second *size function* operating from the control circle to the whole *Rotor sub-grid* area, ending with grid elements of the same size of the corresponding *Wind tunnel sub-grid elements*. An *interior* boundary condition was used for control circle borders, thus ensuring the continuity of the cells on both sides of the mesh.

Some details of the grid are visible in Figures 5 and 6: grid independent solutions were found using an unstructured mesh topology with approximately 10^6 cells. For more information about mesh generation and code validation, see [8] and [9].

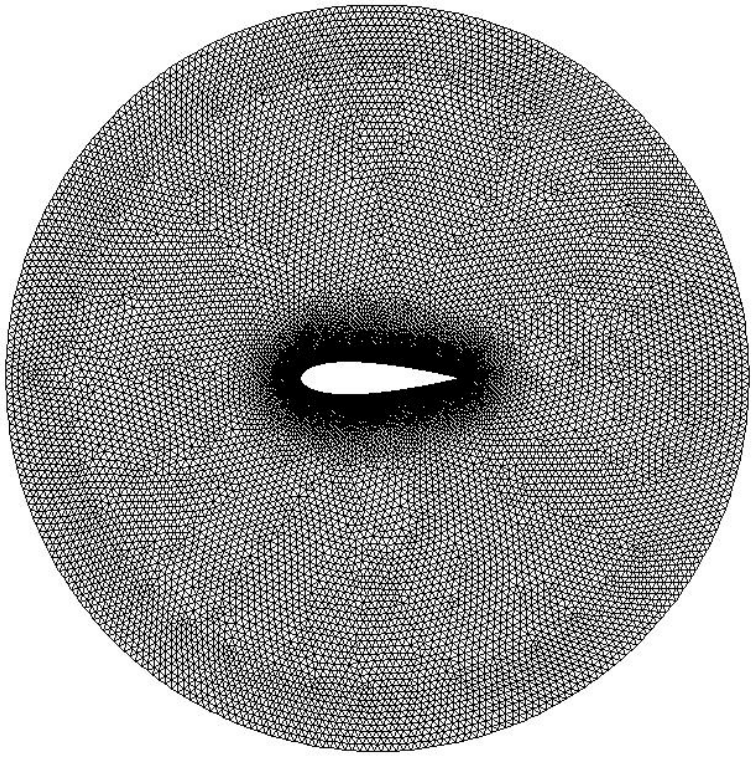

Figure 6: Control circle for NACA 0021 blade section (from: [9])

Temporal Discretization and Convergence Criteria

The commercial CFD package used was ANSYS FLUENT 6.3.26 ®, that implements 2-D Reynolds-averaged Navier-Stokes equations using a finite volume-finite element based solver. The fluid has been assumed to be incompressible, being the maximum fluid velocity in the order of 60 m/s.

The temporal discretization has been achieved by imposing a physical time step equal to the lapse of time the rotor takes to make a 1° rotation. An improved temporal-discretization simulation did not show any significant variation [9].

As a global convergence criterion, each simulation has been run until instantaneous torque coefficient values showed a deviation of less than 1% compared with the

corresponding values of the previous period, corresponding to a rotation of 120° due to rotor three-bladed geometry. Residual convergence criterion for each physical time step has been set to 10^{-5}.

The present simulations required about 16 CPU seconds per physical time step. An average of about 30 sub-iterations have been necessary to converge the solution at each physical time step. The simulations, performed on an 8 processor, 2.33 GHz clock frequency computer, have required a total CPU time of about 16 days for each simulation.

Aerodynamic Noise Simulation

As pointed out by Surugiu and Paraschivoiu [11], wind turbine acoustic emissions can be subdivided in mechanical and aerodynamic:

- mechanical sound is mainly generated by the gearbox, but also by other machine components, such as the generator. As reported by Pedersen [3], in the last 10 years, manufacturers have been able to decrease the mechanical sound to a level below the aerodynamic sound;
- aerodynamic sound is typically the dominating part of wind turbine noise. It comprises a broadband sound (that is a continuous distribution of sound pressure over a frequency range) and an amplitude modulation (when the sound pressure level rises and falls with time). It is generated by the fluctuating aerodynamic components of action (mainly the lift force) on the turbine blades.

The present work concentrates merely on aerodynamic sound: the performance and aeroacoustic analysis is based upon a simplified aerodynamic model, consisting in the representation of flow field characteristics every 4 deg rotor azimuthal position along blade trajectory, as exemplified in Figure 7.

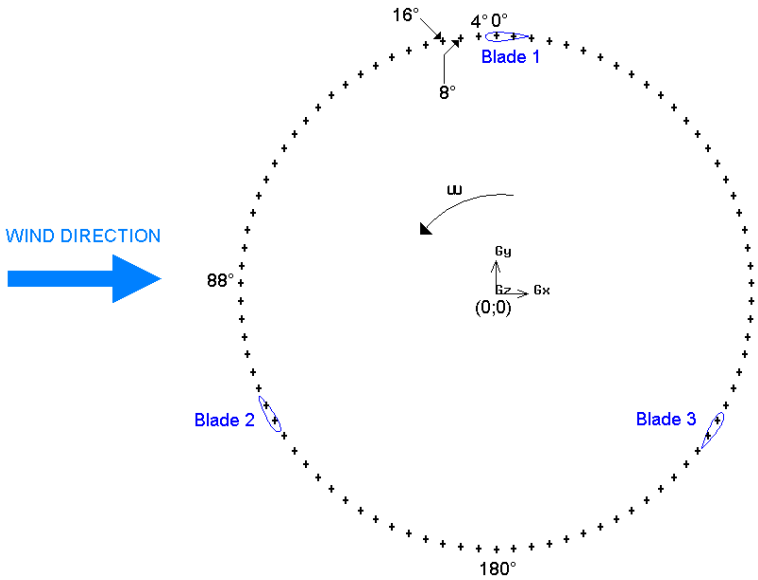

Figure 7: Reference azimuthal position along blade trajectory (from: [8])

After running the simulation until the transient flow field had become statistically steady [12], ANSYS FLUENT far-field method based on the Ffowcs Williams and Hawkings equation and its integral solution was adopted [7]. This acoustic model, based on an inhomogeneous wave equation that can be derived by manipulating the continuity equation and the Navier-Stokes equations, allows to select multiple source surfaces and receivers. The sound pressure signal thus obtained can be processed using the fast Fourier trasform (FFT) and associated postprocessing capabilities to compute and plot quantities such as the overall sound pressure level (SPL) and power spectra.

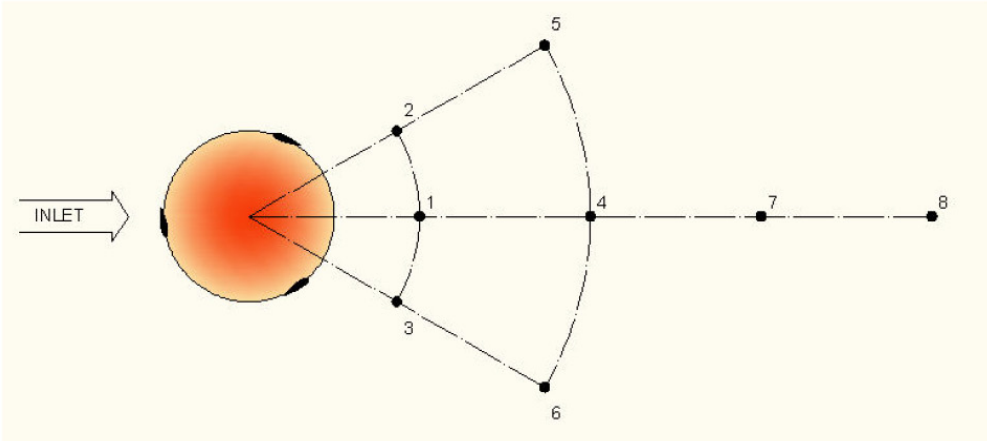

Figure 8: Spatial displacement of the eight acoustic receivers

The spatial coordinates of the acoustic receivers location are summarized in Table 2.

Receiver	x coordinate [mm]	y coordinate [mm]
1	1030	0
2	892	515
3	892	-515
4	2060	0
5	1784	1030
6	1784	-1030
7	3090	0
8	4120	0

Table 2: Spatial coordinates of the acoustic receivers location

Figure 8 represents the location of the eight acoustic receivers displayed inside the computational domain: four of them were placed axially in the wake of the rotor,

spaced one rotor diameter each other, while the other four receivers were displayed aside from the direction of unperturbed wind speed, at an angle of ±30 deg with respect to the rotor axis.

Results and Discussion

Figure 9 represents the evolution of the maximum values of acoustic power level, defined as:

$$L_W = 10 \log_{10} (W_{sound}/W_0) \quad (3)$$

during a full period of revolution (equal to 120 deg, due to rotor three-bladed geometry) as a function of azimuthal position, for an incident wind speed of 9 m/s and an optimum tip speed ratio of 2.33, for both *Model 0* and *Model 1* rotor architectures. Also *Model 0* instantaneous torque coefficient, defined as:

$$C_T(\theta) = \frac{T(\theta)}{1/2\, \rho\, A_s\, R_{rotor}\, V_\infty^2} \quad (4)$$

is represented, allowing a comparison between rotor torque generation and noise emission. As can be clearly seen, the azimuthal positions of maximum torque generation (and, consequently, power, being the rotor operating at constant angular speed) correspond to the azimuthal positions of maximum noise emission. It can also be noticed that instantaneous values of acoustic power level are quite similar for the two analyzed models.

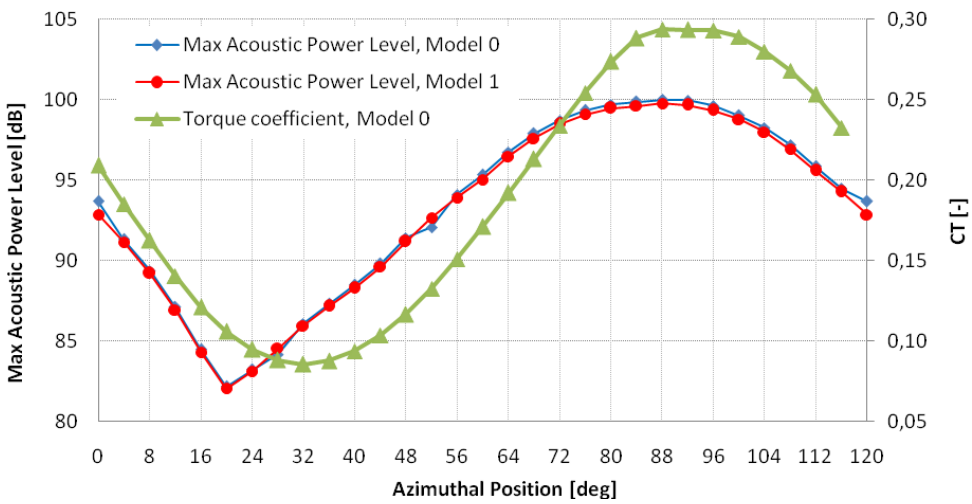

Figure 9: Evolution of the maximum values of acoustic power level (left) and instantaneous torque coefficient (right) for the two analyzed models (being

torque values quite similar, for the sake of clarity just *Model 0* instantaneous values of torque coefficient are represented)

Two relevant azimuthal positions can be identified:

- a peak of noise emission, in correspondence of 88 deg azimuthal position;
- a minimum point of noise emission, in correspondence of 20 deg azimuthal position.

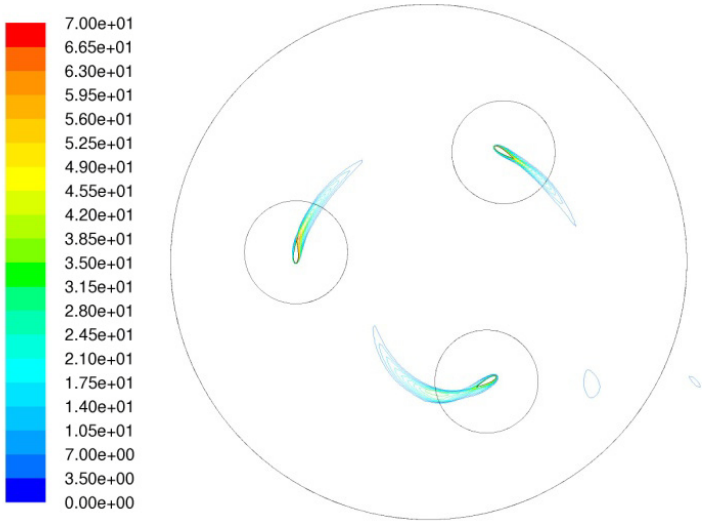

Figure 10: Contours of acoustic power level [dB] in correspondence of 88 deg azimuthal position, *Model 0*

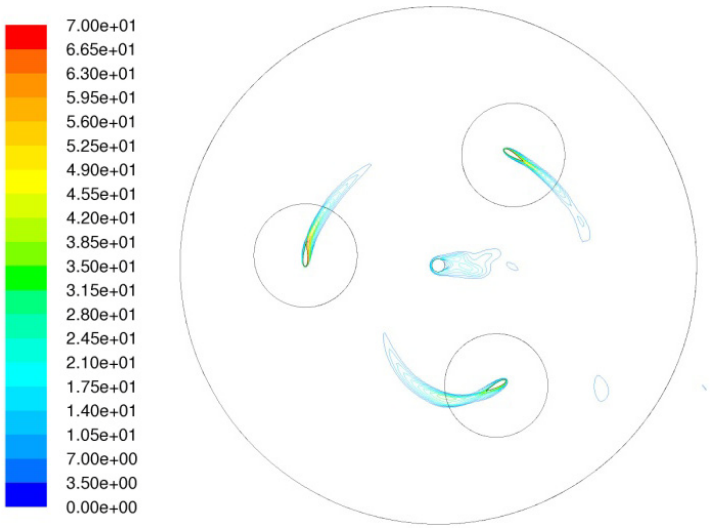

Figure 11: Contours of acoustic power level [dB] in correspondence of 88 deg azimuthal position, *Model 1*

Figures 10 and 11 compare the contours of acoustic power level in correspondence of 88 deg azimuthal position (peak of noise emission) for both *Model 0* and *Model 1* configurations. As can be clearly seen, noise emission during the upwind period of blade revolution (where maximum blade torque values are reached) is quite higher with respect to the downwind one. Once more, it can be noticed that instantaneous values of acoustic power level are quite similar for the two analyzed models, being the noise emission of the central shaft negligible if compared to the noise emission of rotor blades.

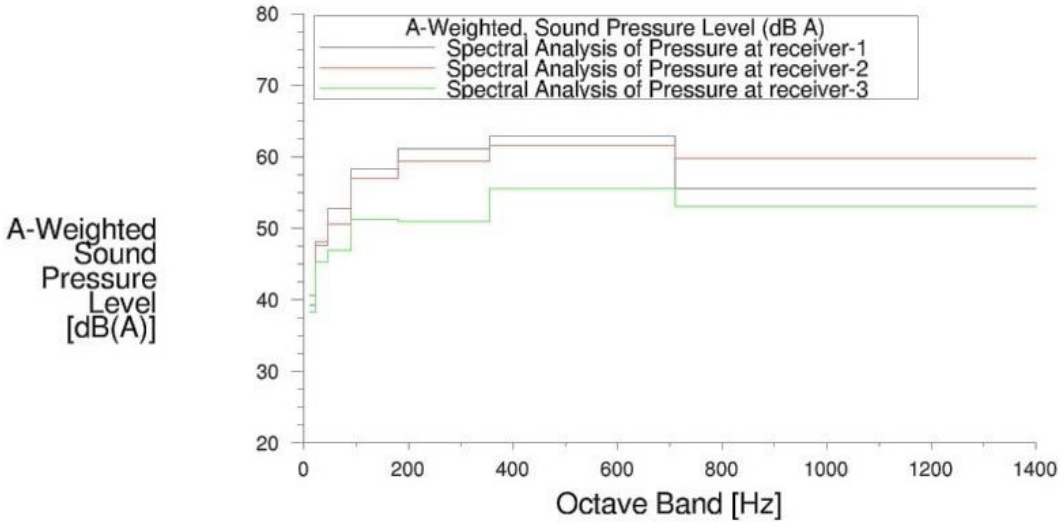

Figure 12: Spectral analysis of sound pressure level for receivers No. 1, 2 and 3 (placed at one diameter distance from rotor axis) in correspondence of 88 deg azimuthal position, *Model 0*

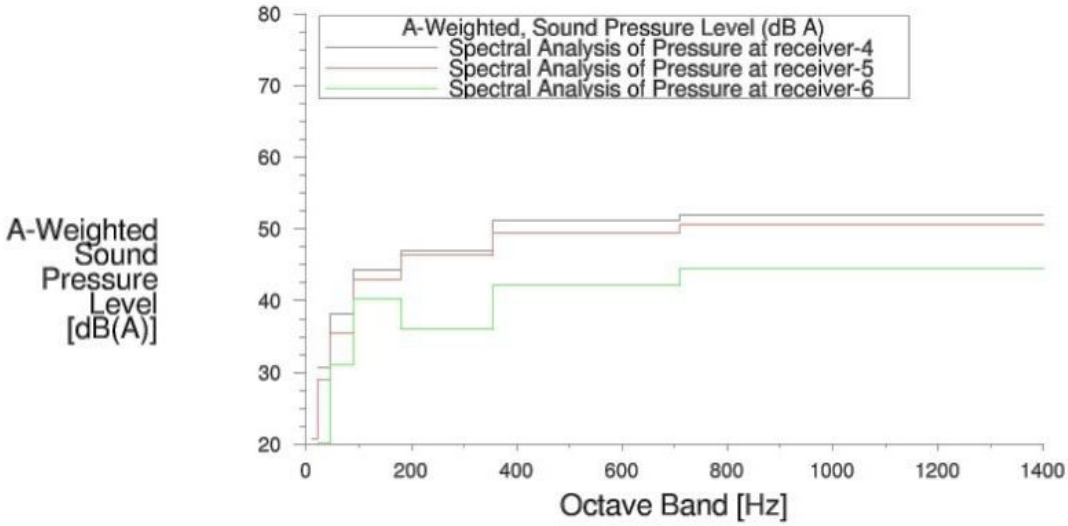

Figure 13: Spectral analysis of sound pressure level for receivers No. 4, 5 and 6 (placed at two diameter distance from rotor axis) in correspondence of 88 deg azimuthal position, *Model 0*

Figures 12 and 13 show the spectral analysis of sound pressure level, defined as:

$$SPL = 20 \log_{10} (p/p_{ref}) \quad (5)$$

for receivers No. 1, 2, 3, 4, 5 and 6 in correspondence of 88 deg azimuthal position (peak of noise emission) for *Model 0* rotor configuration. In order to take into account also the dependence of the sensation of loudness with frequency according to the work of Fletcher and Munson [13], A-frequency weighting was applied to the computed sound pressure level, as schematized in Figure 14.

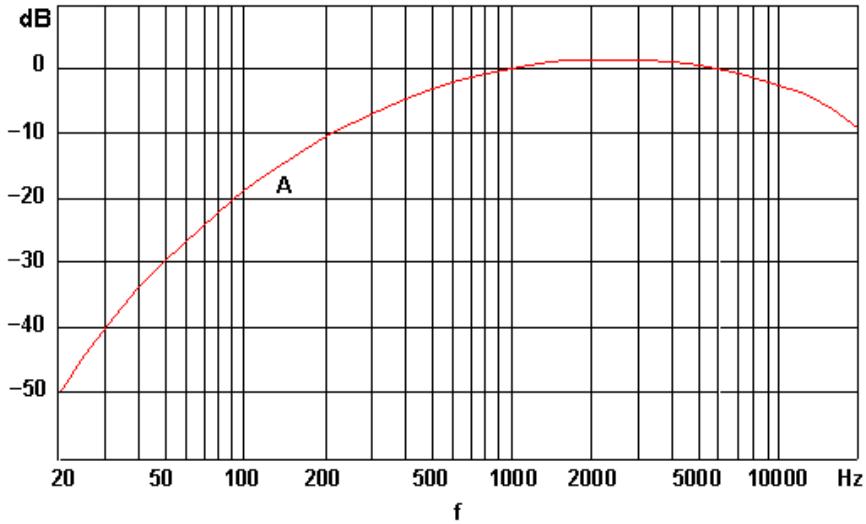

Figure 14: A-frequency weighting contours

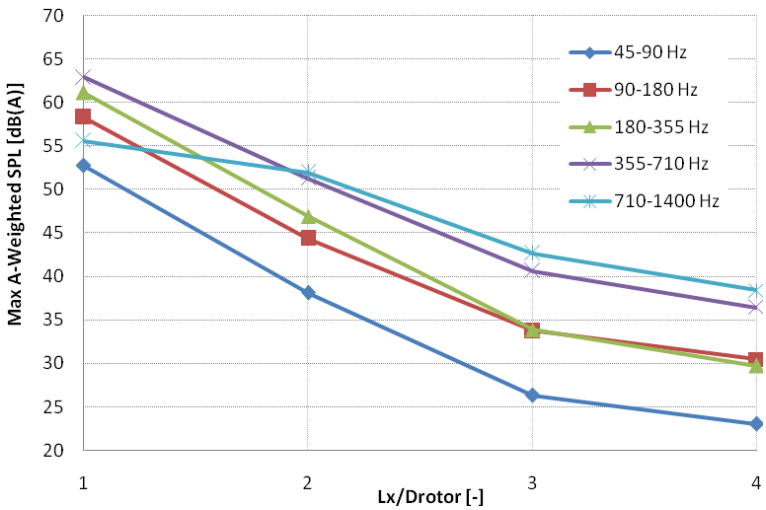

Figure 15: Decrease of A-weighted values of SPL as a function of the non-dimensionalized distance from rotor axis in the direction of unperturbed freestream for several ranges of frequency, *Model 0*

The higher A-weighted SPL can be registered between 350 and 710 Hz for the receivers located at one-diameter distance from rotor axis, being the higher values registered from the receiver (No. 1) placed axially in the wake of the turbine. However, as can be seen in Figure 13, A-weighted SPL values decrease quite dramatically with the distance from rotor axis, at least for lower frequencies (under 710 Hz). This phenomenon can be better seen from Figure 15, showing the decrease of A-weighted values of SPL as a function of the non-dimensionalized distance from rotor axis in the direction of unperturbed freestream for several ranges of frequency.

Figures from 16 to 19 compare the evolution of the maximum values of A-weighted SPL (measured from all of the acoustic receivers displayed inside the computational domain) as a function of azimuthal position during a full period of rotor revolution.

The effect of the central shaft is now dramatically visible: while *Model 0* maximum values of A-weighted SPL are almost constant during the turbine revolution, *Model 1* measured values present marked oscillations as a function of azimuthal position. From Figure 18, a sudden decrease of maximum values of A-weighted SPL is registered from receiver No. 1 in correspondence of 12 deg azimuthal position and a gradual increase to the original value (with respect to *Model 0* calculations) can be seen between 68 and 88 deg azimuthal position.

The described phenomenon is due to the passage of the downwind blade into the wake generated from the rotor shaft, as can be clearly seen from the comparison between Figures 20 and 21, showing the contours of absolute velocity magnitude in corrispondence of 44 deg azimuthal position (as evidenced by the red arrow in Figure 18) for both *Model 0* and *Model 1* rotor configurations.

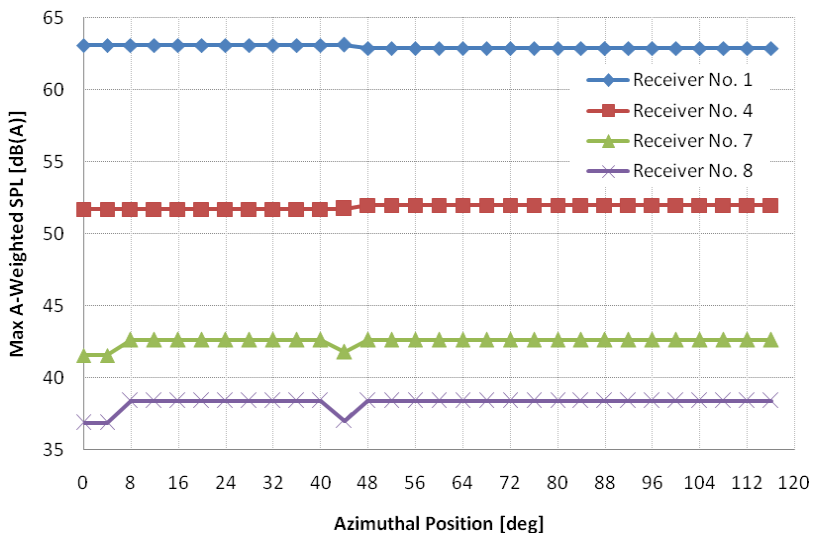

Figure 16: Evolution of the maximum values of A-weighted SPL (measured from receivers No. 1, 4, 7 and 8) as a function of azimuthal position during a full period of rotor revolution, *Model 0*

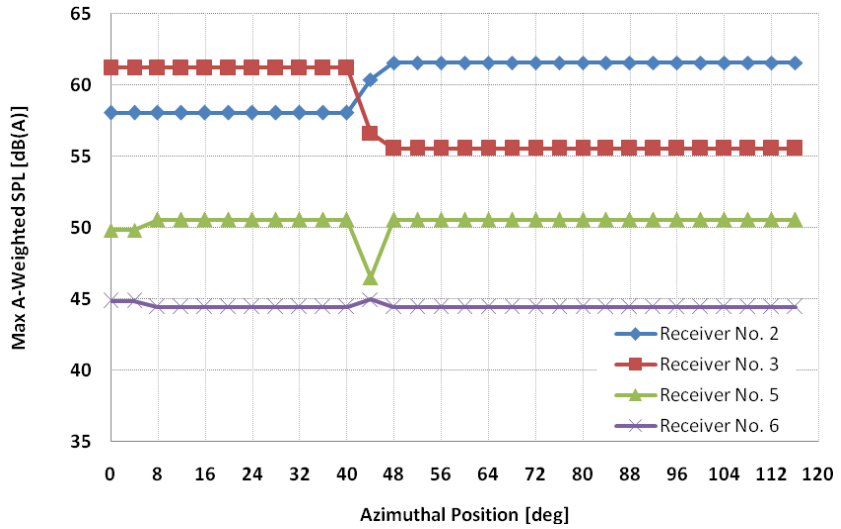

Figure 17: Evolution of the maximum values of A-weighted SPL (measured from receivers No. 2, 3, 5 and 6) as a function of azimuthal position during a full period of rotor revolution, *Model 0*

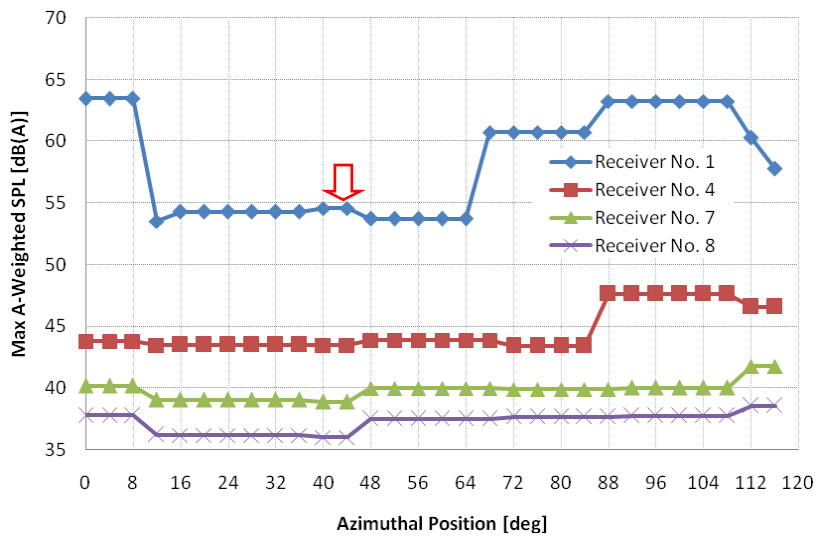

Figure 18: Evolution of the maximum values of A-weighted SPL (measured from receivers No. 1, 4, 7 and 8) as a function of azimuthal position during a full period of rotor revolution, *Model 1* (the red arrow indicates a reference position which will be used in the continuation of the present work)

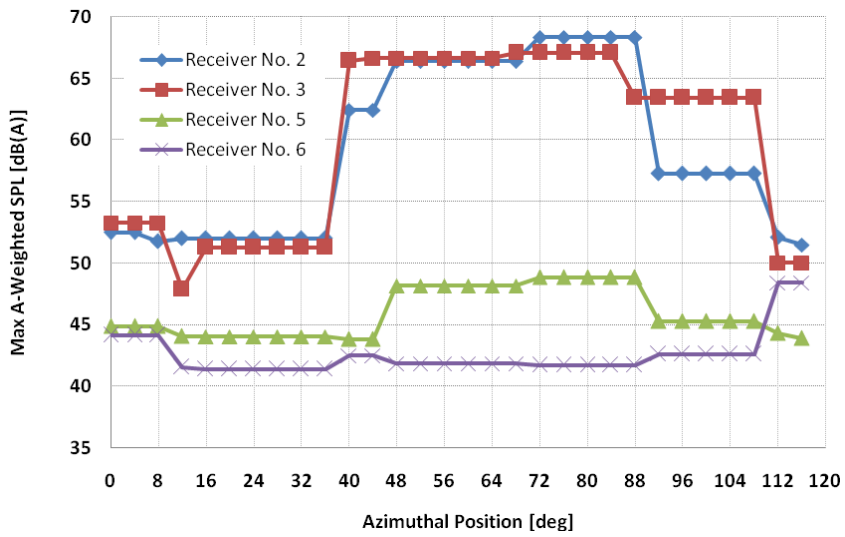

Figure 19: Evolution of the maximum values of A-weighted SPL (measured from receivers No. 2, 3, 5 and 6) as a function of azimuthal position during a full period of rotor revolution, *Model 1*

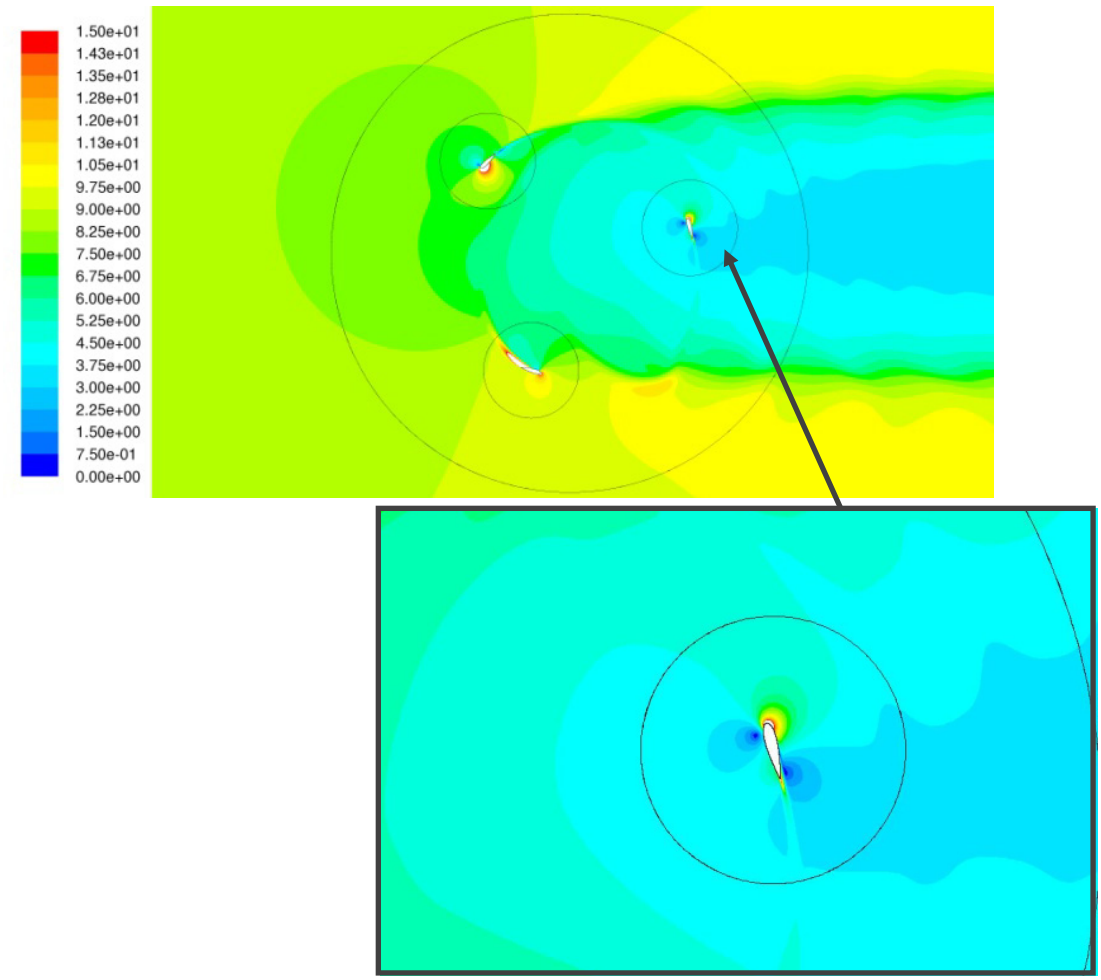

Figure 20: Contours of absolute velocity magnitude [m/s] in correspondence of 44 deg azimuthal position, *Model 0*

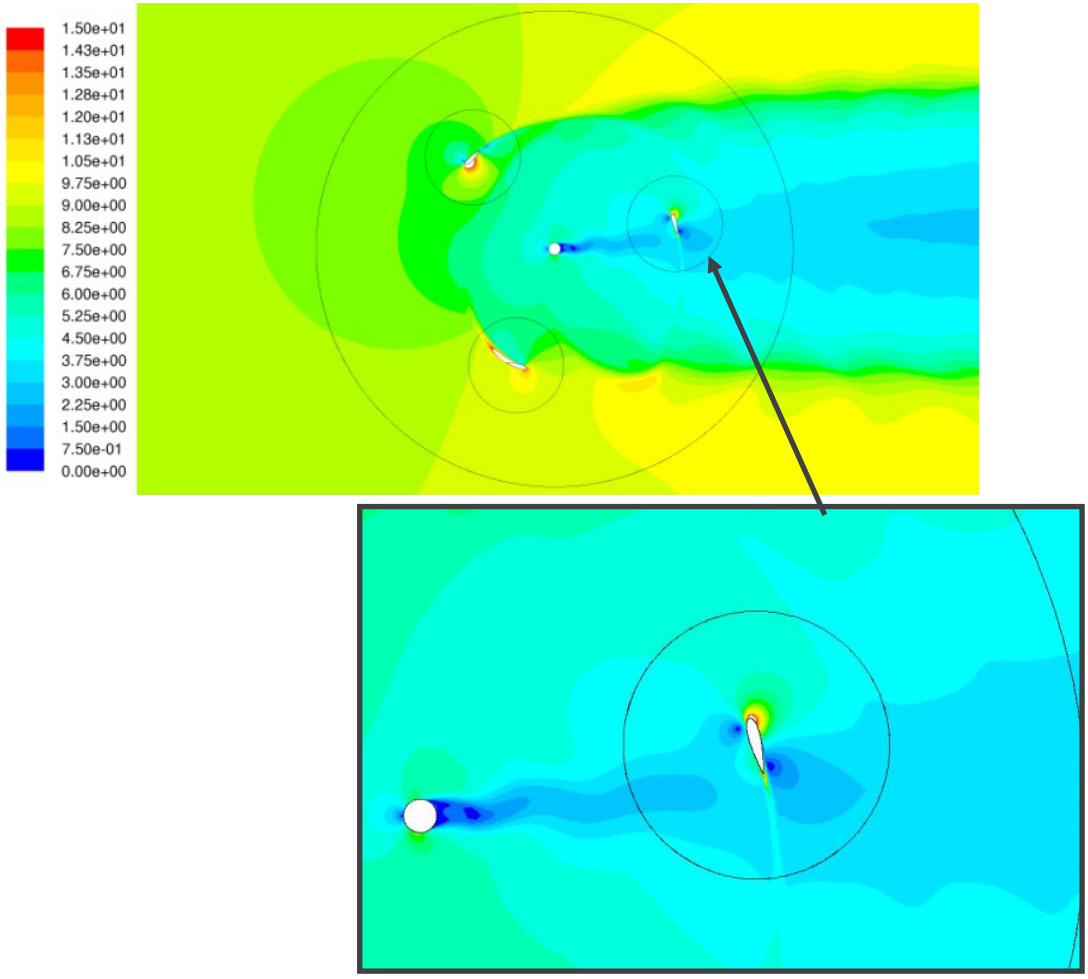

Figure 21: Contours of absolute velocity magnitude [m/s] in correspondence of 44 deg azimuthal position, *Model 1*

The resultant effect of the described phenomenon is a pulsation occurring twice in a period:

- when the downwind blade enters the wake from the central shaft (in correspondence of the sudden decrease of maximum values of A-weighted SPL);
- when the downwind blade exits from the wake from the central shaft (in correspondence of the gradual increase of maximum values of A-weighted SPL).

Being rotor angular velocity, determined from eq. (1), equal to 40.73 rad/s, the corresponding rotor period of revolution can be determined from the following equation:

$$T = \frac{2\pi}{3\omega} = 0.051\,\text{s} \qquad (6)$$

resulting the corresponding acoustic pulsation frequency:

$$f = 2\frac{1}{T} = 39.2\,\text{Hz} \tag{7}$$

Conclusions and Future Works

In this paper, a numerical model for the evaluation of the effect of the central shaft on overall rotor noise emission of a straight-bladed vertical-axis Darrieus wind turbine was presented, based on the application of the Ffowcs-Williams and Hawkings acoustic model.

A simplified aeroacoustic model, based on the analysis of pressure fluctuations at discrete and fixed rotor azimuthal positions along blade trajectory was presented, allowing the correlation between rotor dynamic characteristics, such as torque and power coefficients, and acoustic measurements.

The results of two-dimensional simulations were proposed for a classical NACA 0021 three-bladed rotor design operating at optimum TSR value. The obtained results showed great correspondence between azimuthal positions of maximum torque and power generation and azimuthal positions of maximum noise emission, once again confirming wind turbine noise emission to be strictly connected with power generation. It was also seen that noise emission during the upwind period of blade revolution (where maximum blade torque values are reached) is quite higher with respect to the downwind one.

The obtained results showed also a quite dramatic decrease of A-weighted SPL values with the distance from rotor axis, at least for lower frequencies (under 710 Hz).

The comparative analysis of acoustic power level between two rotor architectures, respectively characterized by the presence and the absence of the central shaft, showed very little difference, resulting the noise emission of the central shaft negligible if compared to the noise emission of rotor blades. On the contrary, the evolution of the maximum values of A-weighted SPL as a function of azimuthal position during a full period of rotor revolution evidenced the dramatic effect of the central shaft, causing marked oscillation in the measured acoustic values due to the passage of the downwind blade into the wake generated from the rotor shaft itself and causing a low frequency pulsation whose period is connected to rotor angular velocity.

Further work is to be performed in order to investigate several freestream velocities and TSR values, allowing a quantification of the effect of the central shaft on noise emission for the full range of rotor operating conditions.

References

[1] Leventhall, G., *Wind Turbine Noise: Perspective for Control*, DEWIMagazin Nr. 27, August 2005, pp. 60-61;

[2] Sezer-Uzol, N., Gupta, A., Long, L. N., *3-D Time-Accurate Inviscid and Viscous CFD Simulations of Wind Turbine Rotor Flow Fields*, Lecture Notes in Computational Science and Engineering, 2009, Vol. 67, pp. 457-464;
[3] Pedersen, E., *Human Response to Wind Turbine Noise – Perception, Annoyance and Moderating Factors*, Doctoral Thesis, Goteborg Universitet, Occupational and Environmental Medicine Department of Public Healt and Community Medicine, The Sahlgrenska Academy, Goteborg, Sweden, 2007;
[4] Caridi, D., *Industrial CFD Simulation of AerodynamicNoise*, PhDThesis, Università degli Studi di Napoli Federico II, 2008;
[5] Timouchev, S., *CFD-CAA Study of Generic Savonius Wind Turbine Rotor*, First International Meeting on Wind Turbine Noise: Perspectives for Control, Berlin, 17th - 18th October 2005;
[6] Iida, A., Mizuno, A., Keiki, F., *Numerical Simulation of Aerodynamic Noise Radiated from Vertical Axis Wind Turbines*, Proceedings of the 18th International Congress on Acoustics ICA 2004, Kyoto International Conference Hall, April 4 to 9, 2004, Kyoto, Japan;
[7] Ffowcs Williams, J. E., Hawkings, D. L., *Sound Generation by Turbulence and Surface in Arbitrary Motion*, Philosophical Transactions of the Royal Society, Series A, Vol. 264, No. 1151, 1969, pp. 321 - 342;
[8] RacitiCastelli, M., Englaro, A., Benini, E., *The Darrieus Wind Turbine: Proposal for a New Performance Prediction Model Based on CFD*, submitted for publication to Energy on December 17, 2010;
[9] RacitiCastelli, M., Pavesi, G., Battisti, L., Benini, E., Ardizzon, G.,: *Modeling Strategy and Numerical Validation for a Darrieus Vertical Axis Micro-Wind Turbine*, ASME 2010 International Mechanical Engineering Congress & Exposition, November 12-18, 2010, Vancouver, British Columbia, Canada, IMECE2010-39548;
[10] Strickland, J. H.: *The Darrieus Turbine: A Performance Prediction Model Using Multiple Streamtube*, SAND75-0431;
[11] Surugiu, L., Paraschivoiu, I, *Acceptability, Environmental and Social Aspects of Wind Energy*, Proceedings of the 1999 European Wind Energy Conference, 1-5 March 1999, Nice, France, James & James (Science Publishers) Ltd, pp. 586-589;
[12] ANSYS FLUENT ® User's Guide, Chapter 21: *Predicting Aerodynamically Generated Noise*, Fluent Inc., 2006;
[13] Fletcher, H., Munson, W. A., *Loudness, its Definition, Measurement and Calculation*, Journal of the Acoustic Society of America 5, 82-108 (1933).